



# Comprehensive Chemistry of HeH<sup>+</sup> in the Early Universe\*

E. D. S. Courtney<sup>1</sup> , R. C. Forrey<sup>2</sup> , R. T. McArdle<sup>1</sup> , P. C. Stancil<sup>1</sup> , and J. F. Babb<sup>3</sup> 

<sup>1</sup> Department of Physics and Astronomy and the Center for Simulational Physics, University of Georgia, Athens, GA 30602, USA; [pstancil@uga.edu](mailto:pstancil@uga.edu)

<sup>2</sup> Department of Physics, Penn State University, Berks Campus, Reading, PA 19610, USA

<sup>3</sup> Institute for Theoretical Atomic, Molecular, and Optical Physics, Center for Astrophysics | Harvard & Smithsonian, Cambridge, MA 02138, USA

Received 2021 February 28; revised 2021 May 6; accepted 2021 May 16; published 2021 September 28

## Abstract

The recent detection of the helium hydride ion (HeH<sup>+</sup>) in the planetary nebula NGC 7027 has inspired studies revisiting the dominant processes for its formation and destruction. Because radiative association is the primary formation mechanism for the helium hydride ion at all redshifts, and many early universe chemistry models rely on accurate results for calculations of destruction rates, we explicitly computed rovibrationally distinguished partial cross sections and rate coefficients of helium hydride formation via radiative association, and modeled the abundance of HeH<sup>+</sup> in the early universe using recently available rate coefficients for all relevant formation and destruction reactions. The rate coefficients for the radiative association formation reaction of HeH<sup>+</sup> and radiative charge transfer in He<sup>+</sup> + H collisions were obtained using two distinct methods. Our newly calculated rate coefficients along with other recently reported He chemistry reactions and updated cosmological parameters were incorporated into a new calculation of the abundance of HeH<sup>+</sup> for redshifts between  $z = 10$  and 4000. We find that the abundance of the helium hydride ion is at least three orders of magnitude larger than previous predictions for redshifts near  $z = 20$ . Rovibrationally distinguished radiative association rate coefficients are given as a function of temperature, and the significance of stimulated radiative association for redshifts  $z > 400$  is also shown.

*Unified Astronomy Thesaurus concepts:* [Early universe \(435\)](#); [Interstellar abundances \(832\)](#); [Molecule formation \(2076\)](#)

*Supporting material:* machine-readable tables

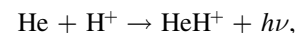
## 1. Introduction

Before the formation of stars in the early universe, low mass atoms and atomic ions formed at the onset of the recombination era. Because the ionization potential of helium is larger than that of atomic hydrogen, helium was the first neutral atom to form, through the combination of He<sup>+</sup> with free electrons, followed quickly by the creation of the helium hydride ion (HeH<sup>+</sup>). As the helium hydride ion's formation and ensuing destruction creates a path to form molecular hydrogen (H<sub>2</sub>), the abundance of which plays a role in gravitational collapse of primordial halos and first star formation, HeH<sup>+</sup> is of interest to studies of the early universe. Although HeH<sup>+</sup> was first observed in the laboratory in 1925 (Hogness & Lunn 1925) and suggested by Lepp & Stancil (1998) to be one of the first molecules to form in the early universe, initiating the start of chemistry, the emission spectrum indicating its presence in interstellar space was not directly observed until 2019 (Güsten et al. 2019; Neufeld et al. 2020).

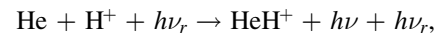
Because of the simplicity of HeH<sup>+</sup>, many studies have investigated the efficiencies for the primary reactions involved in its formation and destruction. Although the predicted rates have varied over time, as better techniques have been applied, HeH<sup>+</sup> has repeatedly been determined to be more abundant than most other primordial molecules, including LiH, H<sub>2</sub><sup>+</sup>, and LiH<sup>+</sup>, increasing its importance in early universe chemistry (Bovino et al. 2011). In order to give a more thorough understanding of the conditions in the early universe, we focus here on improving the accuracy of the formation rate of HeH<sup>+</sup> through radiative association and stimulated radiative association, the related radiative charge transfer process, and modeling

the abundance of HeH<sup>+</sup> in the early universe using the most recently reported reaction data.

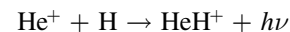
Radiative association is the process by which two gaseous atoms or molecules collide to form a larger molecule while emitting a photon of energy  $h\nu$ ; in the dominant radiative association formation reaction for the helium hydride ion, neutral helium combines with a free proton to form HeH<sup>+</sup>, either spontaneously,



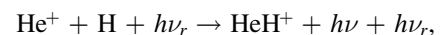
or as the result of stimulation by an incident photon of energy  $h\nu_r$ ,



a process previously calculated to be significant (Stancil & Dalgarno 1998; Zygelman et al. 1998). Here we extend the work of Forrey et al. (2020), who studied



and



by computing final-state resolved rate coefficients for the four listed radiative association processes as well as for the related radiative charge transfer reaction,



Atomic units are used throughout unless otherwise noted.

\* Released on Month Date Year.

## 2. Theoretical Methods

### 2.1. Radiative Association

The rate coefficients for radiative association were obtained as functions of temperature by first calculating the partial cross sections for transitions to bound rovibrational states over six decades of energy, using the known transition dipole moments, ab initio potentials, and the equations given below. The partial cross sections were calculated according to a method that includes both direct and indirect radiative association reactions (Forrey 2013, 2015), and applied to the limiting cases where the gas is assumed to be either in local thermodynamic equilibrium (LTE) or in nonlocal thermodynamic equilibrium in the zero-density limit (NLTE-ZDL). In the NLTE-ZDL, formation is assumed to occur through two-body interactions at zero radiation temperature; realistic astrophysical conditions typically lie between these two limits, but it has been shown that the two limits converge at high temperatures (Cairnie et al. 2017; Forrey et al. 2020).

The partial cross section  $\sigma_{J'}(v'', E)$  is calculated from

$$\sigma_{J'}(v'', E) = \frac{64 \pi^5 \nu^3}{3 c^3 k_b^2} p [J' M_{(v'', J'-1; k', J')}^2 + (J' + 1) M_{(v'', J'+1; k', J')}^2], \quad (1)$$

where  $\nu$  is the photon frequency,  $k'$  is the initial wavevector,  $k_b$  is the Boltzmann constant, and  $p$  is the probability factor in the initial electronic state. Furthermore,  $J'$  is the initial rotational quantum number,  $v'', J''$  are the vibrational and rotational quantum numbers for the final HeH<sup>+</sup> molecule, and  $M$  is the electric transition dipole moment (TDM) element between initial and final states for each transition given by

$$M_{k'J', v''J''} = \int_0^\infty f_{k'J'}(R) D(R) \phi_{v''J''}^n(R) dR, \quad (2)$$

where  $\phi_{v''J''}^n(R)$  is the normalized final radial wave function, the TDM element is denoted as  $D(R)$ , and the nuclear separation is  $R$ . The initial free wave function  $f_{k'J'}(R)$  is normalized such that

$$f_{k'J'}(R) \approx \left( \frac{2\mu}{\hbar^2 \pi k'} \right)^{\frac{1}{2}} \sin(k'R - \frac{1}{2} J' \pi + \eta_{J'}), \quad (3)$$

as  $R \rightarrow \infty$  and where  $k'^2 = \frac{2\mu E}{\hbar^2}$ ,  $\eta_{J'}$  is the phase shift, and  $\mu$  is the reduced mass.

The cross sections calculated in Equation (1) were then summed with the appropriate probability factor  $p$  computed according to the method of Dalgarno et al. (1990) described below. For a given molecular state of spin  $S$  and orbital angular momentum projection quantum number  $N'$ , the probability of approach  $p_{NS}$  is given by

$$p_{NS} = g_{NS} / g_{ab}, \quad (4)$$

where

$$g_{NS} = (2S + 1)(2 - \delta_{0,N}) \quad (5)$$

and

$$g_{ab} = (2L_a + 1)(2S_a + 1)(2L_b + 1)(2S_b + 1). \quad (6)$$

The total number of possible molecular states correlating to the asymptotic atomic states, of total electronic orbital angular momentum  $L_i$  and electron spin  $S_i$ , is given by  $g_{ab}$ , where  $a$  and

$b$  label the colliding species. This probability factor was then used to calculate the total cross section for spontaneous and combined (spontaneous and stimulated) formation reactions,

$$\sigma(E) = \sum_{J'} \sum_{v''} \sigma_{J'}(v'', E). \quad (7)$$

The total or state-resolved cross sections are then used to calculate the spontaneous reaction rate coefficients and the combined reaction rate coefficients as functions of temperature,

$$\alpha(T) = \left( \frac{8}{\mu\pi} \right)^{\frac{1}{2}} \left( \frac{1}{k_b T} \right)^{\frac{3}{2}} \int_0^\infty E \sigma(E) e^{-E/k_b T} dE \quad (8)$$

The rate constant (8) for direct formation is typically computed via numerical integration using the calculated cross section (Equation (7)). An alternative theoretical method, which includes both direct and indirect processes and does not require calculation of the cross section, is to compute the rate constant using the formula

$$\alpha(T) = \frac{P_{NS}}{\hbar Q_T} \sum_{b,u} c_u (2J' + 1) e^{-\beta E_u} \Gamma_{u \rightarrow b}^{\text{rad}}, \quad (9)$$

where  $Q_T = (\mu/2\pi\beta\hbar^2)^{3/2}$  is the translational partition function, and  $\Gamma_{u \rightarrow b}^{\text{rad}}$  is the matrix element for a radiative transition from an unbound state  $u = \{v', J'\}$  of the entrance channel to a bound state  $b = \{v'', J''\}$  of the exit channel. In this formulation, all states are assumed to be unit-normalized energy eigenstates in a Sturmian basis set representation (Forrey 2013, 2015).

For a closed system at constant  $T$ , it is easy to show that  $c_u = 1$  for all states. This is the so-called LTE rate constant. When the system exchanges energy with its surroundings, such as the exiting photons produced by radiative association (RA), the population of resonant unbound states may be nonthermal, and the coefficients in Equation (9) should be computed from the solution of an appropriate master equation. In the limiting NLTE case where there are no excitation mechanisms available to the system, the steady-state solution of the master equation yields

$$c_u = \frac{\Gamma_u^{\text{tun}}}{\Gamma_u^{\text{tun}} + \Gamma_u^{\text{rad}}}, \quad (10)$$

where  $\Gamma_u^{\text{tun}}$  is the tunneling width for the unbound state and  $\Gamma_u^{\text{rad}}$  is the radiative width computed by summing over all possible decay channels. Nonresonant states have  $c_u = 1$  as in the LTE case. Long-lived quasibound states, however, have  $\Gamma_u^{\text{tun}} \ll \Gamma_u^{\text{rad}}$  so  $c_u \rightarrow 0$  and their contribution is effectively removed from the sum in Equation (9). This is the NLTE-ZDL rate constant.

The radiative matrix element includes spontaneous and stimulated emission and may be written as

$$\Gamma_{u \rightarrow b}^{\text{rad}} = \frac{A_{u \rightarrow b}}{1 - e^{-(E_u - E_b)/k_b T}}, \quad (11)$$

for a pure blackbody radiation field with temperature  $T_r$ . The Einstein  $A$  coefficients are given by

$$A_{u \rightarrow b} = \frac{4}{3c^3} (E_u - E_b)^3 S_{J', J''} |\langle u | D | b \rangle|^2, \quad (12)$$

where  $S_{J', J''}$  are the appropriate line strengths. For the  $\Sigma - \Sigma$  transitions considered in the present work, the line strengths are

given by

$$S_{J',J''} = \begin{cases} J' + 1, & J'' = J' + 1 \\ J', & J'' = J' - 1 \end{cases} \quad (13)$$

### 2.2. Radiative Charge Transfer

In the Sturmian formulation, the unbound states are unit-normalized positive energy eigenstates and may be treated on the same footing as bound states. Therefore, the rate constant for radiative charge transfer may be computed using Equation (9) with bound states in the exit channel replaced by unbound states.

### 2.3. Early Universe Chemistry

Accurate calculation of the radiative association rate coefficients are particularly important as models of early universe chemistry often calculate certain destruction rates via detail balance based upon the reverse formation process (Gay et al. 2011). Additionally, radiative association is the primary formation reaction for  $\text{HeH}^+$ , though it reaches its maximum value at approximately  $z = 20$  (Bovino et al. 2011). Similarly, simulated radiative association is most significant for  $2500 > z > 150$ , though its maximum rate is approximately 1% of the spontaneous radiative association rate over this interval (Bovino et al. 2011).

In addition to the radiative association calculations, the abundance of  $\text{HeH}^+$  in the early universe was calculated. As total particle density and temperature are directly correlated with redshift  $z$  (Lepp & Stancil 1998), which is inversely related to time since the big bang,

$$\frac{dt}{dz} = \frac{3.086 \times 10^{17}}{h(1+z)^2(1+\Omega_m z)^{\frac{1}{2}}}, \quad (14)$$

the newly determined rate coefficients were used to calculate the abundance as a function of redshift, where the radiation temperature  $T_r$  is related to redshift by

$$T_r = 2.725(1+z) \text{ K}. \quad (15)$$

Here, we adopt  $h = H_0/100 = 0.6781$  is the Hubble constant in units of  $100 \text{ km s}^{-1} \text{ Mpc}^{-1}$ , and  $\Omega_m = 0.308$  is the total matter density ratio. The hydrogen density is modeled by

$$n_H = 1.123 \times 10^{-5}(1 - Y_p)\Omega_b h^2(1+z)^3 \text{ cm}^{-3}, \quad (16)$$

where  $Y_p = 0.24672$  is the helium mass fraction (Cooke & Fumagalli 2018), and  $\Omega_b = 0.0484$  is the ratio of the baryonic matter density to the critical density (Walker et al. 2018). The matter temperature  $T_m$  model is that adopted in Gay et al. (2011).

In order to calculate the  $\text{HeH}^+$  abundance, we considered nine primary He chemistry formation and destruction reactions, utilizing recently reported rate coefficients, including those calculated or measured by Forrey et al. (2020), Güsten et al. (2019), Novotný et al. (2019), Gay et al. (2011), and Bovino et al. (2011) as listed in Table 1. The newly calculated rate coefficients for spontaneous radiative association were fit to

$$a_1 \left( \frac{T_m}{300 \text{ K}} \right)^{b_1} e^{-\frac{T_m}{c_1}} + a_2 \left( \frac{T_m}{300 \text{ K}} \right)^{b_2} e^{-\frac{T_m}{c_2}}, \quad (17)$$

**Table 1**

Primary Destruction and Formation Reactions of  $\text{HeH}^+$  Updated in the Current Simulations with Their Respective Reactants and Products

Reaction	Reactants	Products
1	$\text{HeH}^+ + \text{H}$	$\text{He} + \text{H}_2^+$
2	$\text{HeH}^+ + e$	$\text{He} + \text{H}$
3	$\text{HeH}^+ + h\nu$	$\text{He} + \text{H}^+$
4	$\text{HeH}^+ + \text{H}_2$	$\text{He} + \text{H}_3^+$
5	$\text{He} + \text{H}^+$	$\text{HeH}^+ + h\nu$
6	$\text{He} + \text{H}^+ + h\nu$	$\text{HeH}^+ + 2h\nu$
7	$\text{He}^+ + \text{H}$	$\text{HeH}^+ + h\nu$
8	$\text{He} + \text{H}_2^+$	$\text{HeH}^+ + \text{H}$
9	$\text{He}^+ + \text{H}$	$\text{He} + \text{H}^+ + h\nu$

**Table 2**

New Fit Coefficients for  $\text{HeH}^+$  Processes in the LTE Limit

Reaction <sup>a</sup>	Fit Equation	Coefficient $a_i$ ( $10^{-20} \text{ cm}^3 \text{ s}^{-1}$ )	$b_i$	$c_i$ (K)
5	17	1.56	-0.374	46,000
		11.8	-0.244	2,890
6 <sup>b</sup>	18	0.130	0.408	36,400
		7.89	-0.399	921
3 <sup>b,c</sup>	18	0	0	...
		500	0.5	20,500

**Notes.**

<sup>a</sup> See Table 1.

<sup>b</sup> Fits assume  $T_r = T_m$ .

<sup>c</sup> The coefficient  $a_2$  has units of  $\text{s}^{-1}$  and the data was taken from Miyake et al. (2011).

or

$$a_1 \left( \frac{T_m}{300 \text{ K}} \right)^{b_1} e^{-\frac{T_m}{c_1}} + a_2 \left( \frac{T_m}{300 \text{ K}} \right)^{b_2} e^{-\frac{c_2}{T_m}}, \quad (18)$$

with the coefficients given in Table 2.

## 3. Results and Discussion

Overall, the newly calculated cross sections and rate coefficients for the radiative association formation reaction are in good agreement with most prior calculations, but also show some new features that have not been previously taken into account. For example, the RA rate constant for  $\text{He} + \text{H}^+$  in Figure 1 shows several curves corresponding to different thermodynamic conditions. The curves labeled NLTE-ZDL agree very well with previous calculations of Zygelman et al. (1998). Additional NLTE-ZDL results (not shown) also agree for other blackbody temperatures reported in the prior work (Zygelman et al. 1998). The new features in the present work are the LTE curves that account for the narrow quasibound resonances in the entrance channel. These resonances provide a significant increase in the LTE rates for  $T_m > 10$  K. Stimulated emission for  $T_r > 0$  is included in the results using Equation (11). Conditions in the early universe correspond most closely to LTE with  $T_r = T_m$ . Figure 1 shows the curve for this case deviates from spontaneous emission ( $T_r = 0$ ) when the common temperature is greater than 300 K. The NLTE-ZDL curve with  $T_r = T_m$  corresponds most closely to what is typically included in models of the early universe. Therefore, replacing the NLTE-ZDL rate with the more appropriate LTE

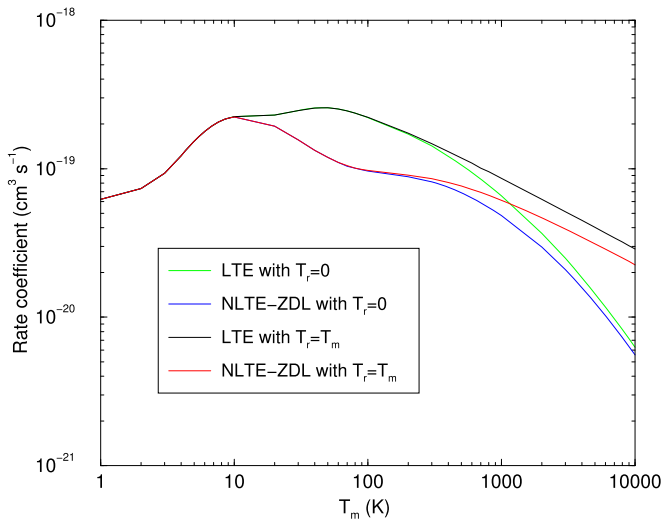


**Figure 1.** Rate coefficients for  $\text{He} + \text{H}^+$  radiative association (combined reactions 5 and 6, see Table 1) as a function of temperature in LTE and NLTE-ZDL. The NLTE-ZDL curves agree with previous results of Zygelman et al. (1998).

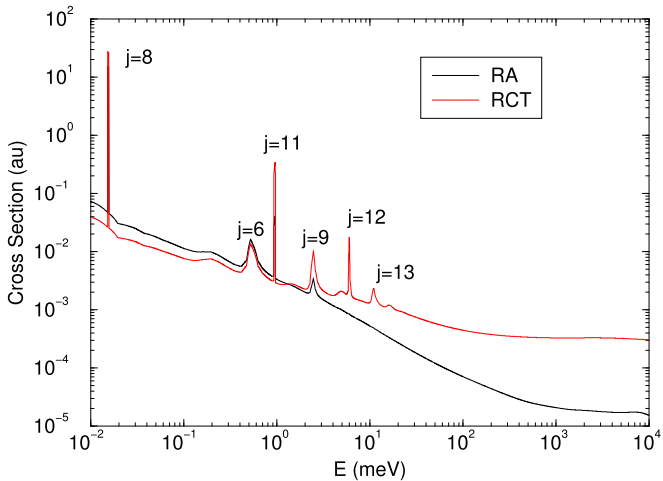


**Figure 2.** Total cross sections for radiative association (RA, reaction 7) and RCT (reaction 9) for  $\text{He}^+ + \text{H}$  collisions. The most narrow resonances ( $J' = 8$  and  $J' = 11$ ) contribute to the LTE rates but are removed from the NLTE-ZDL rates.

rate should provide a small increase in the  $\text{HeH}^+$  abundance at large  $z$ .

A similar study was performed for  $\text{He}^+ + \text{H}$  collisions. The RA and radiative charge transfer (RCT) cross sections are shown in Figure 2. The smooth backgrounds for both processes agree very well with the previous results of Zygelman et al. (1989) and Zygelman & Dalgarno (1990). The resonances are also similar to the previous results, but are not identical due to small differences in the molecular data that was used. Whereas all resonances contribute to the LTE rate, the most narrow resonances ( $J' = 8$  and  $J' = 11$ ) are effectively removed from the NLTE-ZDL rate due to fact that  $c_u$  is negligibly small as computed with Equation (10). The difference between the NLTE-ZDL and LTE rate coefficients is shown in Figure 3, while the agreement with prior RA results were presented in Forrey et al. (2020). The influence of the narrow resonances is very strong at low temperature, but becomes negligible above

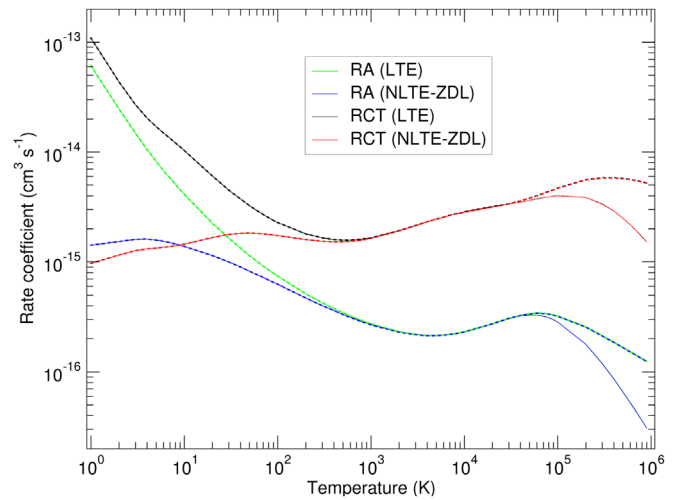


**Figure 3.** Rate coefficients for radiative association (reaction 7) and radiative charge transfer (reaction 9) in the LTE and NLTE-ZDL limits for  $\text{He}^+ + \text{H}$  collisions. The dashed curves include stimulated processes.

1000 K. Stimulated processes are shown to only be important above about 50,000 K.

The strong impact of the two quasibound resonances ( $J' = 8$  and  $J' = 11$ ) on LTE rates at low temperatures suggests bound states of the  $\text{He}^+ + \text{H}$  potential could play a role in the formation of  $\text{HeH}^+$ . We studied the possibility of inverse electronic predissociation to these bound states and found that the rates were very small due to the large exponential decay in the Boltzmann factor and the increasing value of  $Q_T$  at large  $T$ . The Boltzmann factor for inverse electronic predissociation is dominated by the difference in asymptotic energies due to the lower entrance channel. This same factor would need to be applied to the excited asymptotic densities for the RA mechanism, so the processes may be competitive at low temperatures. Therefore, we provide a table of radiative widths for bound-bound A–X transitions (Table 3).

Turning to final-state resolved rate coefficients for reaction 7, Figure 4(a) displays the ground vibrational state  $v'' = 0$  and relevant matter temperature range. The rate coefficient invariably increases as the rotational quantum number  $J''$  increases, with the maximum value being obtained between 40,000 and 80,000 K for all states, tempting one to conclude that the rate coefficient increases as the energy of the bound level nears the top of the potential well. However, in the ground rotational state  $J'' = 0$ , the rate coefficients display more complex behavior as the vibrational quantum number  $v''$  increases as illustrated in Figure 4(b). Because the rate coefficients were calculated for each rovibrational level, it is possible to find the rovibrational level with maximum rate coefficient for each temperature, as shown in Figure 5. Except at the highest temperatures considered here,  $\text{HeH}^+$  is primarily formed in excited rovibrational levels when reaction 7 is considered. Final-state resolved rate coefficients<sup>4</sup> for all  $v''$ ,  $J''$  are given in Tables 4–15.

#### 4. Applications

As shown in Table 1, nine primary  $\text{HeH}^+$  formation and destruction reactions are considered in the calculation for the

<sup>4</sup> All cross section and rate coefficient data can be found on the UGA Molecular Opacity Project website: [www.physast.uga.edu/ugamop](http://www.physast.uga.edu/ugamop).

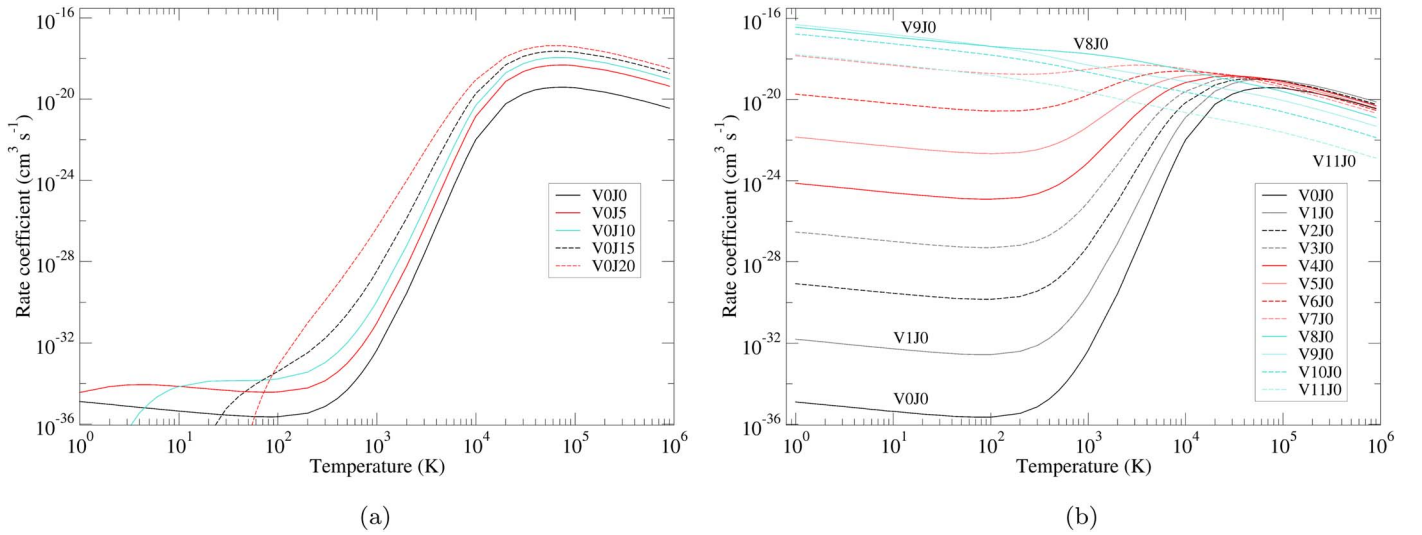


**Figure 4.** Representative  $\text{HeH}^+$  radiative association rate coefficients for  $\text{He}^+ + \text{H}$  as functions of matter temperature  $T_m$  (with  $T_r = 0$ ) calculated for transitions to the indicated rovibrational levels: (a) transitions from the ground vibrational state ( $v'' = 0, J''$ ) and (b) transitions to the ground rotational state ( $v'', J'' = 0$ ).

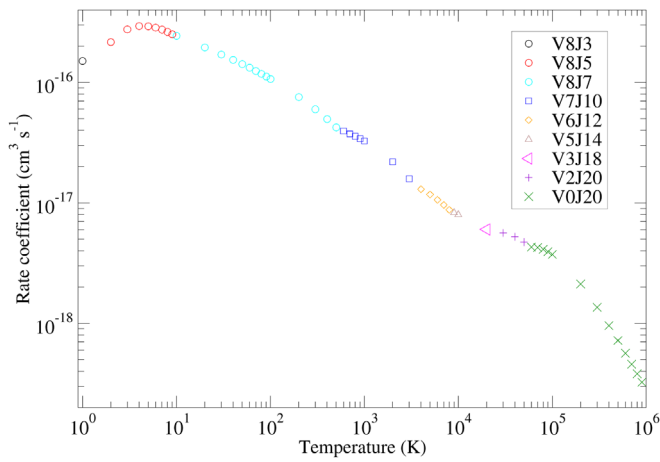


**Figure 5.** The rovibrational levels ( $v'', J''$ ) of  $\text{He}^+ + \text{H}$  (reaction 7) with the maximum rate coefficient at each temperature.

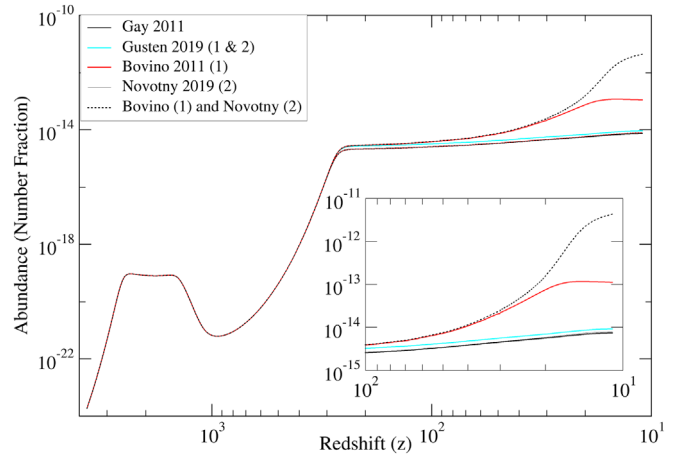


**Figure 6.** Fractional abundance of  $\text{HeH}^+$  in the early universe as a function of redshift, with various reported rates for reactions 1 and 2.

total abundance, including H exchange (1, 4) dissociative recombination (2), photodissociation (3), spontaneous radiative association (5, 7), and stimulated radiative association (6), where  $h\nu$  are photons.

In carrying out the present abundance calculations, the models used by Gay et al. (2011) were used as a starting point and then modified by replacement of specified reaction data with the present data. As shown in Figure 6, adjusting the rates for reactions (1) and (2) primarily affected the abundance at redshifts for  $z < 300$ , unanimously indicating increased abundance compared to calculations made by Gay et al. (2011).

Using the data reported by Bovino et al. (2011) and Novotný et al. (2019) for reactions 1 and 2, respectively, the model shows an increase in abundance of approximately three orders of magnitude from  $10^{-14}$  to  $10^{-11}$ , when compared to the calculations performed with rate coefficients adopted by Güsten et al. (2019) and Gay et al. (2011). The abundances shown in Figure 7 were calculated using the results of Bovino et al. (2011) for reaction (1), Novotný et al.'s (2019) results for reaction (2), and this work's newly calculated results for reactions (5) and (6).

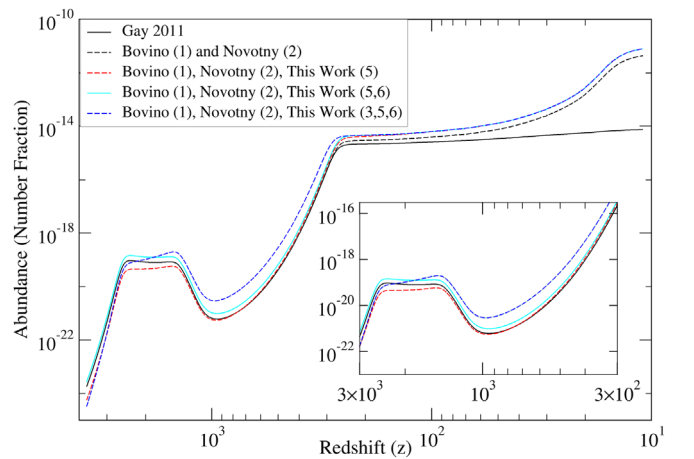


**Figure 7.** Fractional abundance of  $\text{HeH}^+$  plotted as a function of redshift with updated rate coefficients as indicated.

Figure 7 shows that the current radiative association rate coefficients predict an increased abundance of  $\text{HeH}^+$  in the early universe, particularly for redshifts  $z < 200$ , and that

the stimulated radiative association reaction  $\text{He} + \text{H}^+$  is a significant process at redshifts  $z > 400$ , confirming previous findings by Zygelman et al. (1998). Further, using the improved rate coefficient for the exchange reaction 1 increases the  $\text{HeH}^+$  fractional abundance with decreasing  $z$  consistent with the findings of Bovino et al. However, adopting the recent dissociative recombination rate coefficients of Novotny et al. results in a further increase of the  $\text{HeH}^+$  abundance for  $z < 25$ . Finally, prior simulations for the photodissociation process 3 adopted a rate obtained from detailed balance applied to the NLTE-ZDL rate for process 5. In Figure 7 we replace that by an explicit rate calculation for  $\text{HeH}^+$  photodissociation in LTE at  $T_r = T_m$  which results in enhanced  $\text{HeH}^+$  abundances for  $z > 300$ .

Prospects for detecting  $\text{HeH}^+$  in the early universe generally fall within two scenarios: the generation of fluctuations on the cosmic microwave background (CMB) (Maoli et al. 1994) and direct observation of rotational emission lines. Schleicher et al. (2008) revisited the significance of  $\text{HeH}^+$  scattering on CMB photons with a revised chemical network. They predicted  $\text{HeH}^+/\text{H}$  fractional abundances of  $4.3 \times 10^{-15}$  and  $1.0 \times 10^{-14}$  at  $z = 100$  and 10, respectively. They found optical depths of  $10^{-9}$ – $10^{-8}$  from 10–1000 GHz with an expected signal two orders of magnitude below the sensitivity of Planck. The current predicted abundance enhancement in  $\text{HeH}^+$  of 2–3 orders of magnitude in the lower redshift range, due to improvements in the chemistry, may bring the prospects of detecting  $\text{HeH}^+$ -induced fluctuations of CMB anisotropies into reach.

Using the Odin satellite, Persson et al. (2010) performed deep surveys for primordial molecules in the submillimeter, but detected no lines. To interpret their non-detection, Persson et al. (2010) predicted the expected  $\text{HeH}^+$  rotational spectrum as a function of  $z$ . For example, they find the antenna temperatures to be less than  $10^{-8}$  K at  $z = 10$  assuming a  $\text{HeH}^+$  abundance of  $10^{-12}$ . Even with our improved chemistry, the prospects for a direct detection of  $\text{HeH}^+$  rotational lines do not appear promising. A similar conclusion was reached by Kulinich et al. (2020).

## 5. Conclusions and Significance

Recently updated rate coefficients for  $\text{HeH}^+$  radiative association and other He chemistry reactions result in increased  $\text{HeH}^+$  abundance in the early universe compared to previous simulations (Gay et al. 2011). The enhanced abundance at low  $z$  improves the prospect of observing  $\text{HeH}^+$  in the early universe and may effect first star formation through additional cooling (Lepp et al. 2002). The computed final-state resolved radiative association rate coefficients can be adopted in future models which resolve state-to-state reactions. The recent detection of  $\text{HeH}^+$  in the planetary nebulae NGC 7027 (Neufeld et al. 2020) provides hope that the helium hydride molecular ion may be observed in other environments.

This work was partially supported by NSF grant No. PHY-1806180 and NASA grant NNX15AI61G. ITAMP is supported by grant PHY-1521560 from the NSF to Harvard University and the Smithsonian Astrophysical Observatory.

## 6. Supplemental Data Tables

**Table 3**  
Radiative Widths for A–X Transitions of  $\text{HeH}^+$

$J'$	Energy	$A_b$	$A_c$
0	–0.117237-02	0.239079 + 08	0.258937 + 07
0	–0.470281-03	0.114392 + 08	0.254201 + 07
0	–0.129748-03	0.382246 + 07	0.168283 + 07
0	–0.198249-04	0.883347 + 06	0.435868 + 06
0	–0.458353-06	0.549071 + 05	0.275552 + 05

**Note.**  $A_b$ ,  $A_c$  are the summed widths from an initial bound A state with rotational level  $J'$  to all final bound, continuum states of X, respectively. Energy is given in atomic units, radiative widths  $A_b$ ,  $A_c$  are in units of  $\text{s}^{-1}$ , where 0.239079 + 08 represents  $0.239079 \times 10^8 \text{ s}^{-1}$ . Table 3 is published in its entirety in machine-readable format. A portion is shown here for guidance regarding its form and content.

(This table is available in its entirety in machine-readable form.)

**Table 4**  
Rotationally Distinguished Rate Coefficients of  $\text{HeH}^+$  ( $v' = 0, J'$ )

Temperature	$J' = 0$	$J' = 1$	$J' = 2$	$J' = 3$	...
1	1.27–35	3.16–35	5.09–35	5.28–35	...
2	9.28–36	2.52–35	4.19–35	5.33–35	...
3	7.66–36	2.16–35	3.64–35	4.99–35	...
4	6.68–36	1.92–35	3.27–35	4.63–35	...
5	6.01–36	1.75–35	3.00–35	4.32–35	...

**Note.** Temperature is given in Kelvin, rate coefficients are in cubic centimeters per second, where 1.27–35 represents  $1.27 \times 10^{-35} \text{ cm}^3 \text{ s}^{-1}$ . Table 4 is published in its entirety in machine-readable format. A portion is shown here for guidance regarding its form and content.

(This table is available in its entirety in machine-readable form.)

**Table 5**  
Rotationally Distinguished Rate Coefficients of  $\text{HeH}^+$  ( $v' = 1, J'$ )

Temperature	$J' = 0$	$J' = 1$	$J' = 2$	$J' = 3$	...
1	1.56–32	3.89–32	6.28–32	6.54–32	...
2	1.14–32	3.11–32	5.18–32	6.63–32	...
3	9.41–33	2.66–32	4.51–32	6.20–32	...
4	8.21–33	2.37–32	4.05–32	5.76–32	...
5	7.39–33	2.15–32	3.71–32	5.38–32	...

**Note.** Temperature is given in Kelvin, rate coefficients are in cubic centimeters per second. Table 5 is published in its entirety in machine-readable format. A portion is shown here for guidance regarding its form and content.

(This table is available in its entirety in machine-readable form.)

**Table 6**  
Rotationally Distinguished Rate Coefficients of  $\text{HeH}^+$  ( $v' = 2, J'$ )

Temperature	$J' = 0$	$J' = 1$	$J' = 2$	$J' = 3$	...
1	8.53–30	2.13–29	3.45–29	3.62–29	...
2	6.22–30	1.70–29	2.85–29	3.67–29	...
3	5.14–30	1.45–29	2.48–29	3.44–29	...
4	4.48–30	1.29–29	2.23–29	3.20–29	...
5	4.03–30	1.18–29	2.04–29	2.98–29	...

**Note.** Temperature is given in Kelvin, rate coefficients are in cubic centimeters per second. Table 6 is published in its entirety in machine-readable format. A portion is shown here for guidance regarding its form and content.

(This table is available in its entirety in machine-readable form.)

**Table 7**  
Rotationally Distinguished Rate Coefficients of  $\text{HeH}^+$  ( $v' = 3, J'$ )

Temperature	$J' = 0$	$J' = 1$	$J' = 2$	$J' = 3$	...
1	2.95–27	7.40–27	1.20–26	1.27–26	...
2	2.15–27	5.92–27	9.98–27	1.30–26	...
3	1.78–27	5.06–27	8.69–27	1.22–26	...
4	1.55–27	4.50–27	7.80–27	1.13–26	...
5	1.39–27	4.10–27	7.15–27	1.05–26	...

**Note.** Temperature is given in Kelvin, rate coefficients are in cubic centimeters per second. Table 7 is published in its entirety in machine-readable format. A portion is shown here for guidance regarding its form and content.

(This table is available in its entirety in machine-readable form.)

**Table 8**  
Rotationally Distinguished Rate Coefficients of  $\text{HeH}^+$  ( $v' = 4, J'$ )

Temperature	$J' = 0$	$J' = 1$	$J' = 2$	$J' = 3$	...
1	7.41–25	1.86–24	3.05–24	3.27–24	...
2	5.40–25	1.48–24	2.53–24	3.34–24	...
3	4.45–25	1.27–24	2.20–24	3.13–24	...
4	3.88–25	1.13–24	1.97–24	2.91–24	...
5	3.49–25	1.03–24	1.81–24	2.72–24	...

**Note.** Temperature is given in Kelvin, rate coefficients are in cubic centimeters per second. Table 8 is published in its entirety in machine-readable format. A portion is shown here for guidance regarding its form and content.

(This table is available in its entirety in machine-readable form.)

**Table 9**  
Rotationally Distinguished Rate Coefficients of  $\text{HeH}^+$  ( $v' = 5, J'$ )

Temperature	$J' = 0$	$J' = 1$	$J' = 2$	$J' = 3$	...
1	1.38–22	3.50–22	5.80–22	6.28–22	...
2	1.01–22	2.80–22	4.80–22	6.44–22	...
3	8.35–23	2.39–22	4.18–22	6.05–22	...
4	7.28–23	2.13–22	3.76–22	5.63–22	...
5	6.54–23	1.94–22	3.44–22	5.26–22	...

**Note.** Temperature is given in Kelvin, rate coefficients are in cubic centimeters per second. Table 9 is published in its entirety in machine-readable format. A portion is shown here for guidance regarding its form and content.

(This table is available in its entirety in machine-readable form.)

**Table 10**  
Rotationally Distinguished Rate Coefficients of  $\text{HeH}^+$  ( $v' = 6, J'$ )

Temperature	$J' = 0$	$J' = 1$	$J' = 2$	$J' = 3$	...
1	1.85–20	4.69–20	7.82–20	8.56–20	...
2	1.35–20	3.75–20	6.49–20	8.83–20	...
3	1.11–20	3.21–20	5.65–20	8.31–20	...
4	9.70–21	2.85–20	5.08–20	7.73–20	...
5	8.71–21	2.59–20	4.65–20	7.22–20	...

**Note.** Temperature is given in Kelvin, rate coefficients are in cubic centimeters per second. Table 10 is published in its entirety in machine-readable format. A portion is shown here for guidance regarding its form and content.

(This table is available in its entirety in machine-readable form.)

**Table 11**  
Rotationally Distinguished Rate Coefficients of  $\text{HeH}^+$  ( $v' = 7, J'$ )

Temperature	$J' = 0$	$J' = 1$	$J' = 2$	$J' = 3$	...
1	1.44–18	3.65–18	6.06–18	6.62–18	...
2	1.04–18	2.91–18	5.04–18	6.89–18	...
3	8.64–19	2.49–18	4.40–18	6.50–18	...
4	7.52–19	2.21–18	3.95–18	6.05–18	...
5	6.75–19	2.01–18	3.62–18	5.64–18	...

**Note.** Temperature is given in Kelvin, rate coefficients are in cubic centimeters per second. Table 11 is published in its entirety in machine-readable format. A portion is shown here for guidance regarding its form and content.

(This table is available in its entirety in machine-readable form.)

**Table 12**  
Rotationally Distinguished Rate Coefficients of  $\text{HeH}^+$  ( $v' = 8, J'$ )

Temperature	$J' = 0$	$J' = 1$	$J' = 2$	$J' = 3$	...
1	3.67–17	9.16–17	1.46–16	1.50–16	...
2	2.67–17	7.32–17	1.22–16	1.59–16	...
3	2.19–17	6.25–17	1.06–16	1.50–16	...
4	1.91–17	5.55–17	9.59–17	1.40–16	...
5	1.71–17	5.04–17	8.78–17	1.30–16	...

**Note.** Temperature is given in Kelvin, rate coefficients are in cubic centimeters per second. Table 12 is published in its entirety in machine-readable format. A portion is shown here for guidance regarding its form and content.

(This table is available in its entirety in machine-readable form.)

**Table 13**  
Rotationally Distinguished Rate Coefficients of  $\text{HeH}^+$  ( $v' = 9, J'$ )

Temperature	$J' = 0$	$J' = 1$	$J' = 2$	$J' = 3$	...
1	4.93–17	1.11–16	1.41–16	9.64–17	...
2	3.57–17	8.87–17	1.18–16	1.05–16	...
3	2.93–17	7.56–17	1.03–16	1.01–16	...
4	2.54–17	6.68–17	9.32–17	9.42–17	...
5	2.27–17	6.05–17	8.51–17	8.78–17	...

**Note.** Temperature is given in Kelvin, rate coefficients are in cubic centimeters per second. Table 13 is published in its entirety in machine-readable format. A portion is shown here for guidance regarding its form and content.

(This table is available in its entirety in machine-readable form.)

**Table 14**  
Rotationally Distinguished Rate Coefficients of  $\text{HeH}^+$  ( $v' = 10, J'$ )

Temperature	$J' = 0$	$J' = 1$	$J' = 2$	$J' = 3$
1	1.71–17	3.92–17	5.00–17	3.05–17
2	1.24–17	3.13–17	4.20–17	3.33–17
3	1.01–17	2.66–17	3.67–17	3.17–17
4	8.83–18	2.36–17	3.29–17	2.95–17
5	7.90–18	2.14–17	3.00–17	2.75–17

**Note.** Temperature is given in Kelvin, rate coefficients are in cubic centimeters per second. Table 14 is published in its entirety in machine-readable format. A portion is shown here for guidance regarding its form and content.

(This table is available in its entirety in machine-readable form.)

**Table 15**  
Rotationally Distinguished Rate Coefficients of  $\text{HeH}^+$  ( $v' = 11, J'$ )

Temperature	$J' = 0$	$J' = 1$
1	1.67–18	2.52–18
2	1.21–18	2.01–18
3	9.96–19	1.72–18
4	8.64–19	1.52–18
5	7.72–19	1.38–18

**Note.** Temperature is given in Kelvin, rate coefficients are in cubic centimeters per second. Table 15 is published in its entirety in machine-readable format. A portion is shown here for guidance regarding its form and content.

(This table is available in its entirety in machine-readable form.)

## ORCID iDs

E. D. S. Courtney  <https://orcid.org/0000-0002-0154-6940>  
R. C. Forrey  <https://orcid.org/0000-0001-6687-5481>  
R. T. McArdle  <https://orcid.org/0000-0001-5672-0064>  
P. C. Stancil  <https://orcid.org/0000-0003-4661-6735>  
J. F. Babb  <https://orcid.org/0000-0002-3883-9501>

## References

- Bovino, S., Tacconi, M., Gianturco, F., & Galli, D. 2011, *A&A*, 529, A140  
Cairnie, M., Forrey, R. C., Babb, J. F., & Stancil, P. C. 2017, *MNRAS*, 471, 2481  
Cooke, R. J., & Fumagalli, M. 2018, *NatAs*, 2, 957  
Dalgarno, A., Du, M., & You, J. 1990, *ApJ*, 349, 675  
Forrey, R. C. 2013, *PhRvA*, 88, 052709  
Forrey, R. C. 2015, *JChPh*, 143, 024101  
Forrey, R. C., Babb, J. F., Courtney, E. D. S., McArdle, R. T., & Stancil, P. C. 2020, *ApJ*, 898, 86  
Gay, C. D., Stancil, P. C., Lepp, S., & Dalgarno, A. 2011, *ApJ*, 737, 44  
Güsten, R., Wiesemeyer, H., Neufeld, D., et al. 2019, *Natur*, 568, 357  
Hogness, T. R., & Lunn, E. 1925, *PhRv*, 26, 44  
Kulinich, Y., Novosyadlyj, B., Shulga, V., & Han, W. 2020, *PhRvD*, 101, 083519  
Lepp, S., & Stancil, P. C. 1998, in *Molecular Astrophysics of Stars and Galaxies*, ed. T. W. Hartquist & D. A. Williams (Oxford: Clarendon Press), 37  
Lepp, S., Stancil, P. C., & Dalgarno, A. 2002, *JPhB*, 35, 57  
Maoli, R., Melchiorri, F., & Tosti, D. 1994, *ApJ*, 425, 372  
Miyake, S., Gay, C. D., & Stancil, P. C. 2011, *ApJ*, 735, 21  
Neufeld, D. A., Goto, M., Geballe, T. R., et al. 2020, *ApJ*, 894, 37  
Novotný, O., Wilhelm, P., Paul, D., et al. 2019, *Sci*, 365, 676  
Persson, C. M., Maoli, R., Encrenaz, P., et al. 2010, *A&A*, 515, A72  
Schleicher, D. R. G., Galli, D., Palla, F., et al. 2008, *A&A*, 490, 521  
Stancil, P. C., & Dalgarno, A. 1998, *FaDi*, 109, 61  
Walker, K. M., Porter, R. L., & Stancil, P. C. 2018, *ApJ*, 867, 152  
Zygelman, B., & Dalgarno, A. 1990, *ApJ*, 365, 239  
Zygelman, B., Dalgarno, A., Kimura, M., & Lane, N. F. 1989, *PhRvA*, 40, 2340  
Zygelman, B., Stancil, P. C., & Dalgarno, A. 1998, *ApJ*, 508, 151